Magnetodielectric effects in *A*-site cation-ordered chromate spinels $LiMCr_4O_8$ (M = Ga and In)

Rana Saha,[1] Francois Fauth,[2] Maxim Avdeev,[3] Paula Kayser,[4] Brendan J. Kennedy,[4] and A. Sundaresan[1,*]

[1]*Chemistry and Physics of Materials Unit and International Centre for Materials Science, Jawaharlal Nehru Centre for Advanced Scientific Research, Jakkur P.O., Bangalore 560 064, India*

[2]*CELLS–ALBA synchrotron, E-08290 Cerdanyola del Vallès, Barcelona, Spain*

[3]*Australian Nuclear Science and Technology Organisation, Lucas Heights, New South Wales 2234, Australia*

[4]*School of Chemistry, The University of Sydney, Sydney, New South Wales 2006, Australia*

(Received 7 March 2016; revised manuscript received 18 July 2016; published 15 August 2016)

We report the occurrence of a magnetodielectric effect and its correlation with structure and magnetism in the *A*-site ordered chromate spinel oxides $LiMCr_4O_8$ (M = Ga, In). In addition to magnetic and dielectric measurements, temperature dependent synchrotron and neutron diffraction experiments have been carried out for the Ga compound. The results are compared and contrasted with that of a corresponding conventional *B*-site magnetic chromate spinel oxide, $ZnCr_2O_4$. Like $ZnCr_2O_4$, the *A*-site ordered chromate spinels exhibit a magnetodielectric effect at the magnetic ordering temperature ($T_N \sim 13$–15 K), resulting from magnetoelastic coupling through a spin Jahn-Teller effect. While the presence of a broad magnetic anomaly, associated with a short-range magnetic ordering ($T_{SO} \sim 45$ K) in $ZnCr_2O_4$, does not cause any dielectric anomaly, a sharp change in dielectric constant has been observed in $LiInCr_4O_8$ at the magnetic anomaly, which is associated with the opening of a spin gap ($T_{SG} \sim 60$ K). Contrary to the In compound, a broad dielectric anomaly exists at the onset of short-range antiferromagnetic ordering ($T_{SO} \sim 55$ K) in $LiGaCr_4O_8$. The differences in dielectric behavior of these compounds have been discussed in terms of breathing distortion of the Cr_4 tetrahedra.

DOI: 10.1103/PhysRevB.94.064420

I. INTRODUCTION

Chromium containing spinels, ACr_2X_4 (X = O, S, Se) have emerged as an important class of materials in the study of magnetoelectric and multiferroic properties because some of them undergo magnetic ordering at low temperatures with complex spin structures that results from their frustrated magnetic interactions [1–4]. One such frustrated magnet is the family of *B*-site magnetic spinel oxides of general formula ACr_2O_4 crystallizing in a cubic structure with the space group $Fd\bar{3}m$. In these materials the nonmagnetic ions, occupying the tetrahedral *A* site, form a diamondlike lattice, whereas the Cr^{3+} ions, located at the octahedral *B* site, form a corner-sharing network of Cr_4 tetrahedra, the so-called pyrochlore lattice [5,6]. Unlike the ABO_3 perovskite, where the BO_6 octahedra are connected by vertices and the magnetic exchange occurs through cation-anion-cation superexchange interactions, the magnetic interactions in the *B*-site magnetic spinels involve direct cation-cation, $Cr^{3+}(3d^3) - Cr^{3+}(3d^3)$, interactions as the CrO_6 octahedra are shared by edges [7]. The antiferromagnetic nearest neighbor interaction between neighboring Cr^{3+} ions located on the pyrochlore sublattice gives rise to a strong geometric magnetic frustration [8,9]. To relieve this frustration, ACr_2O_4 undergoes a spin Jahn-Teller effect [10–12] through magnetoelastic coupling, where the structural distortion removes the spin degeneracy, resulting in the development of long-range antiferromagnetic ordering at low temperatures [5,13]. The magnetostructural transition involving the magnetoelastic coupling leads to the concurrent change in crystallographic and magnetic symmetry, which brings about interesting magnetoelectric properties [14,15].

The spinel structure offers a great amount of scope for substitution of different cations at both the *A* and *B* sites and thus enables researchers to tailor various interesting properties. In the conventional *B*-site chromate spinel oxide, for example in $ZnCr_2O_4$, the nonmagnetic Zn^{2+} ions are located at the noncentrosymmetric tetrahedral site ($8a$) with local symmetry T_d, and the Cr^{3+} ions are located at the centrosymmetric site ($16d$) with rhombohedral symmetry D_{3d}. By substituting two inequivalent cations with different oxidation states, Li^+ and Ga^{3+} (In^{3+}), at the *A* site, a different type of frustrated pyrochlore lattice has been made recently [16–18]. These two inequivalent cations exert different amounts of chemical pressures on the Cr_4 tetrahedra, resulting in an alternate arrangement of small and large Cr_4 tetrahedra in a corner-sharing geometry, thereby making a breathing pyrochlore lattice where both Cr-Cr distance alternation and geometrical frustration coexist [17]. Further, the incorporation of two different ions at the *A* site results in the loss of inversion symmetry and thus leads to a reduction of crystal symmetry to $F\bar{4}3m$, where the *A*-cations Li^+ and Ga^{3+} (In^{3+}) occupy the $4a$ and $4d$ Wyckoff positions, respectively, and the Cr^{3+} ions are located at the noncentrosymmetric $16e$ position. In a recent theoretical study it has been suggested that *A*-site cation ordering in chromate spinel oxides can give rise to a local electric dipole moment at the *B*-site magnetic ion, which is located in a local polar noncentrosymmetric surrounding of oxygen ions with C_{3v} symmetry, contributing to the linear magnetoelectric coupling [19]. According to this theoretical prediction, this effect will result in single-ion contribution to the linear magnetoelectric coupling if the resulting spin structure allows it, since spin-orbit coupling modifies the local electric dipole moment of the *B*-site magnetic ion resulting in spin dependent macroscopic electric polarization [20]. In fact, it has recently been demonstrated that the *A*-site magnetic spinels where the magnetic ions are located at the local noncentrosymmetric site indeed exhibits linear magnetoelectric effect [21]. This motivated us to investigate the detailed structural,

*sundaresan@jncasr.ac.in

magnetic, and magnetoelectric properties of the A-site ordered spinel oxides $LiMCr_4O_8$ (M = Ga, In). It is known that the In compound undergoes separate magnetic and structural transitions around 13–16 K and exhibits a broad magnetic anomaly (~60 K) which has been attributed to the opening of a pseudo spin gap [16]. In the case of the Ga compound, it has been suggested that the broad magnetic anomaly around 55 K is related to short-range antiferromagnetic ordering and that magnetostructural transition occurs at low temperature [22].

We observe a dielectric anomaly in both the A-site ordered spinel oxides, $LiMCr_4O_8$ (M = Ga, In) at the magnetostructural phase transition temperatures ($T_{MS} \sim 13$–15 K) similar to that observed in $ZnCr_2O_4$. Interestingly, the compound $LiInCr_4O_8$ shows a sharp dielectric anomaly at the onset of a spin-gap transition at $T_{SG} \sim 60$ K in zero magnetic field, which has been attributed to relatively stronger breathing distortion of the pyrochlore lattice, a unique feature in three-dimensional frustrated pyrochlore networks. On the other hand, a broad dielectric anomaly is observed at the short-range magnetic ordering temperature ($T_{SO} \sim 55$ K) in $LiGaCr_4O_8$. Contrary to the expectation, neither the Ga nor In compounds exhibit a detectable linear magnetoelectric effect at the magnetic ordering temperatures. Neutron diffraction analysis of $LiGaCr_4O_8$ at low temperature (4 K) reveals the coexistence of a tetragonal (28%) and untransformed cubic phase. The magnetic structures associated with these two crystallographic phases, possessing $k_t = (1/2\,1/2\,1/2)$ and $k_c = (001)$, do not allow a linear magnetoelectric effect in $LiMCr_4O_8$ [23].

II. EXPERIMENTS

Polycrystalline samples of A-site ordered $LiMCr_4O_8$ (M = Ga, In) were prepared by conventional solid state reaction method following the procedures reported in Ref. [17], except that the samples in the present study are sintered at a slightly lower temperature (1050 °C). For the sake of comparison, we have prepared $ZnCr_2O_4$ by the solid state route. Phase purities of all these samples were confirmed by analyzing the x-ray diffraction (XRD) data collected with a PANalytical Empyrean diffractometer using Cu Kα_1 monochromatic x-ray radiation. The FullProf Suite program was used for the treatment of diffraction data and Rietveld refinement [24]. The synchrotron XRD data were collected in the angular range 5–45°, using x rays at two different wavelengths of 0.4127 and 0.4959 Å at the Material Science Powder Diffraction Beamline (BL04-MSPD) of the ALBA synchrotron facility [25,26]. Low temperatures were achieved using a recently developed ^{1}He flow cryostat. A temperature dependent neutron diffraction experiment was carried out at the high resolution Echidna diffractometer of the Australian Nuclear Science and Technology Organisation using two different wavelengths of 1.62 and 2.44 Å [27].

Magnetization (dc) measurements were carried out using a superconducting quantum interference device (SQUID) magnetometer, Magnetic Property Measurement System (MPMS)-3, (Quantum Design, USA) in the temperature range of 2–390 K. The temperature dependent specific heat (C_p) was measured between the temperature range of 2 and 80 K in a Physical Property Measurement System (PPMS; Quantum Design, USA). Capacitance and the pyroelectric current measurements were performed with a LCR meter (Agilent E4980A) and an electrometer (Keithley 6517A), respectively, using a multifunction probe inserted in the PPMS, which allowed access to variable temperatures and magnetic fields. The electrodes were made by applying conducting Ag paint on both sides of the thin pellets and drying under an infrared lamp. The capacitance was measured with and without an applied magnetic field while warming after performing the magnetic field (or zero magnetic field) cooling of the sample from 100 K. Before measuring the pyroelectric current, the sample was poled magnetoelectrically from a temperature above T_N and then cooled to the lowest temperature at which the electrodes were short circuited for 15 minutes to remove any stray charges, but the magnetic field was not removed. Then the magnetoelectric current was measured on warming the sample to a temperature above T_N at a rate of 15 K min^{-1} while keeping the magnetic field on. The dc voltage was applied on the samples using a Radiant Technologies Inc. precision workstation.

III. RESULTS AND DISCUSSION

Rietveld analysis of the room temperature XRD pattern demonstrated that compounds $LiGaCr_4O_8$ and $LiInCr_4O_8$ have cubic structure with the space group $F\bar{4}3m$, confirming the ordering of the Li^+ and Ga^{3+} (In^{3+}) cations at the A site of the spinel structure. While there exists only one Cr-Cr distance (2.944 Å) in the conventional $ZnCr_2O_4$ spinel oxide, the A-site ordered compounds have two distinct Cr-Cr distances, 2.830 (2.891) Å and 2.999 (3.057) Å, which correspond to smaller and larger Cr_4 tetrahedra for the Ga (In) compounds, respectively. From the aforementioned distances, it is clear that the Cr-Cr distance in the smaller tetrahedra for both the Ga and In compounds is smaller than the Cr-Cr distance (2.944 Å) in $ZnCr_2O_4$, indicating the stronger direct overlap between t_{2g} orbitals of Cr^{3+} ions, thereby strengthening the magnetic exchange interaction in the Ga and In compounds compared with the Zn compound. On the other hand, the Cr-Cr distance in the larger tetrahedra for the Ga compound is intermediate between the Cr-Cr distance in $ZnCr_2O_4$ (2.944 Å) and $CdCr_2O_4$ (3.035 Å) [28], while for the In compound, this is close to the Cr-Cr distance in $HgCr_2O_4$ (3.056 Å) [29], which indicates relatively weaker magnetic interactions among the larger Cr_4 tetrahedra. In other words, the smaller Cr_4 tetrahedron becomes more isolated in the In compound compared with the Ga compound, demonstrating that the ordering of cations at the A site causes a breathing distortion of the Cr_4 tetrahedra that depends on the size of the trivalent A-site cations [17].

Analysis of temperature dependent synchrotron XRD patterns in $LiGaCr_4O_8$ revealed that the cubic structure ($F\bar{4}3m$) remains unchanged down to the antiferromagnetic ordering temperature ($T_N \sim 14.5$ K). Figure 1(a) shows the room temperature synchrotron XRD pattern of $LiGaCr_4O_8$ obtained from the Rietveld refinement. Analysis of the synchrotron XRD pattern at 5 K [Fig. 1(b)] showed the coexistence of two crystallographic phases ($F\bar{4}3m$ and $I\bar{4}m2$), indicating an incomplete structural phase transformation. This is in contrast to $ZnCr_2O_4$ where the room temperature phase

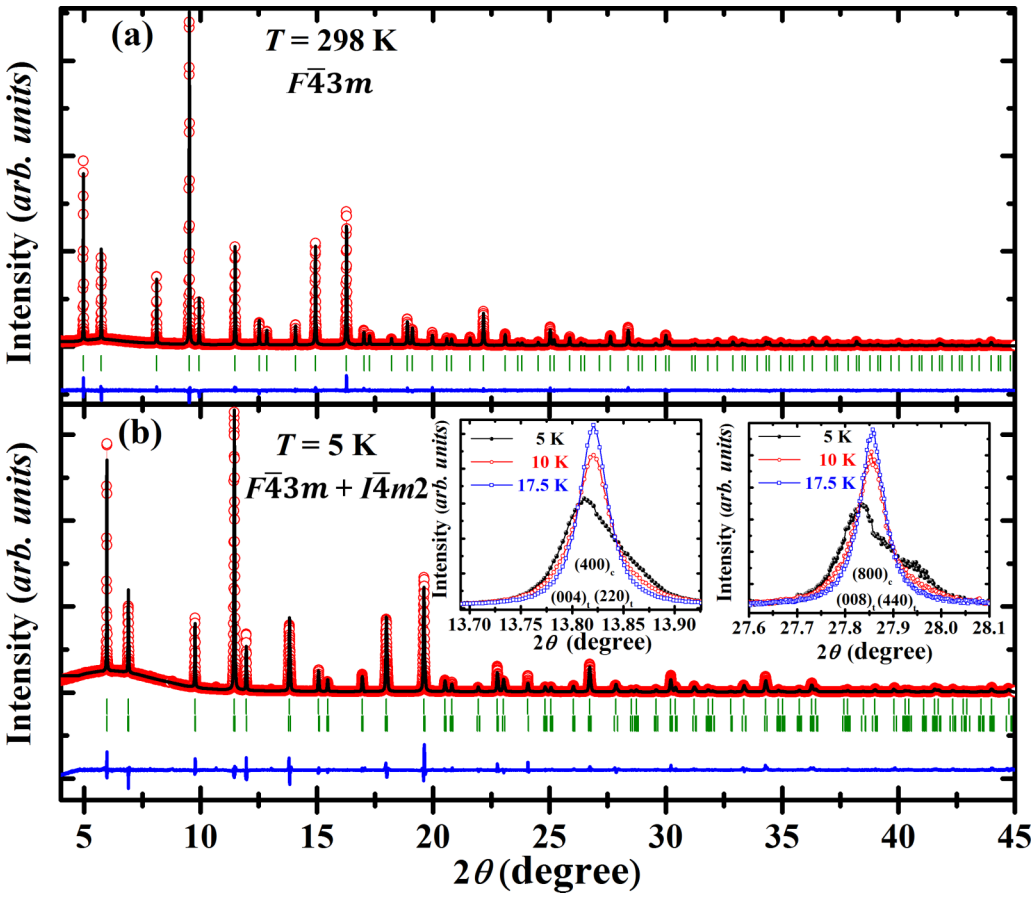

FIG. 1. (a, b) Rietveld refinements on the synchrotron XRD pattern of $LiGaCr_4O_8$ acquired at 298 and 5 K with $\lambda = 0.4127$ and 0.4959 Å, respectively. Red open circle and black solid line are the experimental data and calculated patterns, respectively; green vertical bars indicate the nuclear Bragg reflections, and the blue line below is the difference between the experimental and calculated patterns. The first and second green vertical bars in panel (b) correspond to the Bragg reflections for the cubic and tetragonal phases, respectively. Insets of panel (b) show the broadening and splitting of the two cubic Bragg reflections (400) and (800) in the antiferromagnetic state. The XRD patterns shown in the inset are recorded with $\lambda = 0.4959$ Å. The suffixes *c* and *t* stand for cubic and tetragonal symmetry, respectively. Small unrefined peaks visible in the 2θ range of 7–15 degrees originated from the cryostat.

completely transforms below T_N but to a mixture of two new phases, namely, tetragonal ($I4_1/amd$) and orthorhombic ($Fddd$) [5]. From the refinement of structural parameters, we see that the transformed $I\bar{4}m2$ phase has a c/a ratio of 1.42, which is consistent with the tetragonal distortion of the high temperature cubic phase. Further, it is seen from the XRD pattern at 5 K that the (400) and (800) Bragg peaks are broadened and split, as shown in the inset of Fig. 1(b), indicating the coexistence of strain and lowering of crystal symmetry to tetragonal. The development of large strain, due to the lattice mismatch between the two crystallographic phases, could inhibit complete structural phase transformation and thus result in the coexistence of the two phases at low temperature [30].

To investigate the magnetic and crystallographic structures in detail, we have carried out neutron diffraction experiments on $LiGaCr_4O_8$ at 298 and 4 K. The lattice parameter, obtained from the Rietveld analysis of the room temperature neutron data, is $a = 8.2457$ Å, and we obtain two distinct Cr-Cr distances (2.824 and 3.006 Å), which is in agreement with those obtained from the analysis of the XRD data. Based on Rietveld refinement against the room temperature neutron data, we see full occupancy of Li and Ga ions at their respective sites. Consequently, we fixed the occupancy for the refinements against the low temperature (4 K) neutron data, which is shown in Fig. 2(a). Though we do not see a clear peak splitting in the low temperature (4 K) neutron diffraction data, due to the relatively poorer resolution compared with synchrotron XRD data, it could be modeled considering a mixture of two different space groups, $F\bar{4}3m$ and $I\bar{4}m2$, as inferred from the analysis of synchrotron XRD pattern. It should be mentioned here that such a phase coexistence has been reported recently in $LiInCr_4O_8$ from the analysis of neutron diffraction data at 2 K [16]. The lattice parameters obtained from the refinement of the neutron data for $LiGaCr_4O_8$ at 4 K are $a = 8.2401(3)$ Å for the cubic phase and $a = 5.8123(3)$ Å, $c = 8.2661(3)$ Å for the tetragonal phase. The weight fraction of the tetragonal phase obtained from the refinement for $LiGaCr_4O_8$ is 28(6)% at 4 K, while it is reported to be 70% for $LiInCr_4O_8$ at 2 K [16]. The presence of different phase fractions could be attributed to the difference in the ionic radii of Ga^{3+} (0.47 Å) and In^{3+} (0.62 Å), exerting different amounts of chemical pressure, leading to structural distortion and lowering of crystallographic symmetry to a different extent. The structural

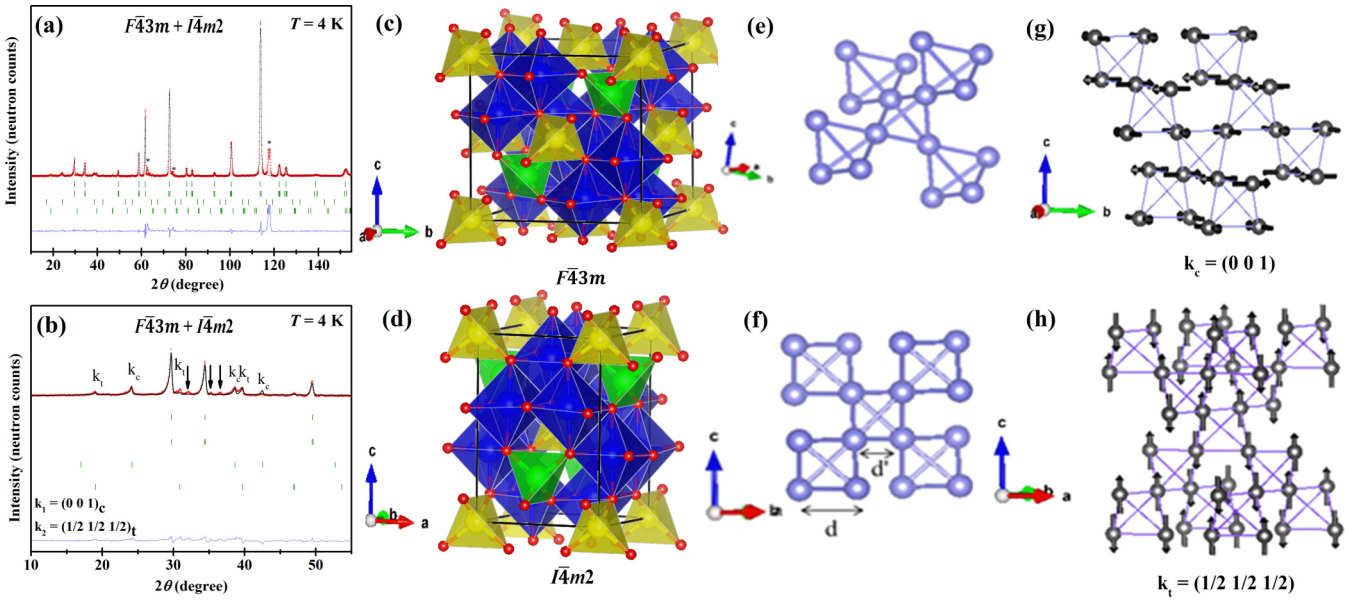

FIG. 2. (a, b) Rietveld refinements on the neutron diffraction pattern of $LiGaCr_4O_8$ acquired at 4 K with $\lambda = 2.4395$ Å for the whole region and small region, respectively, where red cross and black solid line are the experimental data and calculated patterns, green vertical bars indicate the Bragg reflections and the blue line below is the difference between experimental and calculated pattern. The first series of Bragg reflections correspond to the cubic $F\bar{4}3m$ phase and the second correspond to the tetragonal $I\bar{4}m2$ phase, the third and the fourth series account for the magnetic phases for the cubic phase $k_c = (001)$ and for the tetragonal phase $k_t = (1/2\,1/2\,1/2)$, respectively. (*Aluminum peaks from the cryostat). (c, d) Schematic representation of cubic ($F\bar{4}3m$) and tetragonal ($I\bar{4}m2$) structure of $LiGaCr_4O_8$ obtained from the Rietveld refinement on neutron diffraction pattern collected at 4 K, where yellow and green tetrahedra contains the Li^+ and Ga^{3+} ions, respectively, and blue octahedra contains the Cr^{3+} ions. (e, f) Pyrochlore network consists of Cr_4 tetrahedra embedded in the cubic structure and breathing distortion in a three-dimensional network of corner-sharing Cr tetrahedra forming pyrochlore sublattice ($d > d'$). (g) The k_c magnetic structure associated with cubic symmetry, with alternating spin chains on the ab plane. Every second ab plane is rotated 90° with respect to the first. (h) The k_t magnetic structure associated with tetragonal symmetry with chains of spins with two-up and two-down arrangement along the [100] and [010] directions.

parameters of $LiGaCr_4O_8$ obtained from the refinements of the 4 K neutron diffraction data are summarized in Table I. From the structural parameters, obtained from the refinement against the neutron diffraction data, we have drawn the schematics of cubic and tetragonal crystal structures as shown in Figs. 2(c) and 2(d), respectively. In Figs. 2(e) and 2(f) we show, respectively, the schematics of the pyrochlore network made of Cr atoms and two different sizes of the tetrahedral units of the pyrochlore block tuning the magnetic frustration.

TABLE I. Structural parameters of $LiGaCr_4O_8$ obtained from the Rietveld refinement of neutron diffraction pattern acquired at 4 K.

$LiGaCr_4O_8$ (space group: $F\bar{4}3m$), $\lambda = 2.44$ Å Cubic phase fraction = 72 (7) %					
Atom	x	y	z	B_{iso} (Å^2)	Occupancy
Li (4a)	0	0	0	2.3 (5)	1.0
Ga (4d)	0.75	0.75	0.75	0.2 (1)	1.0
Cr (16e)	0.3728 (7)	0.3728 (7)	0.3728 (7)	0.94 (9)	1.0
O1 (16e)	0.1360 (3)	0.1360 (3)	0.1360 (3)	0.05 (6)	1.0
O2 (16e)	0.6175 (3)	0.6175 (3)	0.6175 (3)	0.05 (7)	1.0
$LiGaCr_4O_8$ (space group: $I\bar{4}m2$), $\lambda = 2.44$ Å Tetragonal phase fraction = 28 (6) %					
Atom	x	y	z	B_{iso} (Å^2)	Occupancy
Li (2a)	0	0	0	2.3 (5)	1.0
Ga (2d)	0.0	0.5	0.75	0.2 (1)	1.0
Cr (8i)	0.264 (3)	0	0.873(3)	0.94 (9)	1.0
O1 (8i)	0.284(1)	0	0.634(8)	0.05 (6)	1.0
O2 (8i)	0.251(1)	0	0.108(1)	0.05 (7)	1.0

Magnetic structures associated with both the cubic and tetragonal phases of $LiGaCr_4O_8$ have been identified based on the indexing of the low angle magnetic Bragg peaks in the neutron diffraction pattern [Fig. 2(b)]. For both phases, the magnetic structure determination has been accomplished following the representation analysis technique of group theory described by Bertaut [31]. The basis vectors associated with each possible magnetic model have been obtained with the BasIreps software of the FullProf Suite package [24]. The irreducible representations and the basis vectors are summarized in Table II. A propagation vector, $k_c = (001)$, accounts for the magnetic reflections due to the cubic phase. Among the possible magnetic modes compatible with the space group symmetry and the propagation vector, the best agreement with the experimental data corresponds to the irreducible representation Γ_1. As seen in Fig. 2(g), the magnetic structure can be described as having alternating spin chains along the [110] direction, with every second ab plane rotated 90 degrees with respect to the first one. The magnetic moment of the Cr^{3+} cations in the cubic phase is 0.77(2) μ_B. The lower value of magnetic moment may be due to stronger geometrical frustration in the cubic phase, which remains even below the magnetic ordering temperature. The

TABLE II. Basis vectors for (a) $k_c = (001)$ and the 16*e* site of the cubic space group, $F\bar{4}3m$, and (b) $k_t = (1/2\,1/2\,1/2)$ and the 8*i* site of the tetragonal space group, $I\bar{4}m2$ ($LiGaCr_4O_8$).

(a)	Cr1($x\,x\,x$)	Cr2 ($-x\,-x\,x$)	Cr3($-x\,x\,-x$)	Cr4($x\,-x\,-x$)
Γ_1	(1,−1,0)	(−1,1,0)	(−1,−1,0)	(1,1,0)
Γ_2	(1,1,0)	(−1,−1,0)	(−1,1,0)	(1,−1,0)
	(0,0,1)	(0,0,1)	(0,0,−1)	(0,0,−1)
Γ_3	(1,−1,0)	(−1,1,0)	(1,1,0)	(−1,−1,0)
Γ_4	(1,1,0)	(−1,−1,0)	(1,−1,0)	(−1,1,0)
	(0,0,1	(0,0,1)	(0,0,1)	(0,0,1)
Γ_5	(1,0,0)	(1,0,0)	(−1,0,0)	(−1,0,0)
	(0,1,0)	(0,1,0)	(0,1,0)	(0,1,0)
	(0,0,1)	(0,0,−1)	(0,0,−1)	(0,0,1)
	(0,−1,0)	(0,−1,0)	(0,1,0)	(0,1,0)
	(−1,0,0)	(−1,0,0)	(−1,0,0)	(−1,0,0)
	(0,0,−1)	(0,0,1)	(0,0,−1)	(0,0,1)
(b)	Cr1($x\,0\,z$)	Cr2 ($-x\,0\,z$)	Cr3($0\,-x\,-z$)	Cr4($0\,x\,-z$)
Γ_1	(1,0,0)	(−1,0,0)	(0,1,0)	(0,−1,0)
	(0,1,0)	(0,−1,0)	(−1,0,0)	(1,0,0)
	(0,0,1)	(0,0,1)	(0,0,1)	(0,0,1)
Γ_2	(1,0,0)	(−1,0,0)	(0,−1,0)	(0,1,0)
	(0,1,0)	(0,−1,0)	(1,0,0)	(−1,0,0)
	(0,0,1)	(0,0,1)	(0,0,−1)	(0,0,−1)
Γ_3	(1,0,0)	(1,0,0)	(0,−i,0)	(0,−i,0)
	(0,1,0)	(0,1,0)	(i,0,0)	(i,0,0)
	(0,0,1)	(0,0,−1)	(0,0,−i)	(0,0,i)
Γ_4	(1,0,0)	(1,0,0)	(0,i,0)	(0,i,0)
	(0,1,0)	(0,1,0)	(−i,0,0)	(−i,0,0)
	(0,0,1)	(0,0,−1)	(0,0,i)	(0,0,−i)

magnetic structure of the tetragonal phase is described by the propagation vector $k_t = (1/2\,1/2\,1/2)$ as reported for $LiInCr_4O_8$ [16]. After testing the different solutions given in Table II, the best spin arrangement compatible with the tetragonal space group $I\bar{4}m2$ is given by basis vector 3 of Γ_2. The obtained magnetic moment of the Cr^{3+} cations, aligned along the *c* axis, is 2.33(9) μ_B. The reduction of this value with respect to the expected magnetic moment ($S = 3/2$) might be due to covalence effects. Figure 2(h) shows the magnetic structure of the tetragonal phase of $LiGaCr_4O_8$, consisting of chains with a two-up and two-down spin arrangement along the [100] and [010] directions.

Figures 3(a) and 3(b) show the temperature dependence of dc magnetization, $M\ (T)$, for $LiGaCr_4O_8$ and $LiInCr_4O_8$, respectively. In both compounds a broad maximum is observed around 55–60 K followed by a decrease in the magnetization value near T_N, similar to that observed in $ZnCr_2O_4$. However, the origin of this maximum has been suggested to differ in these *A*-site ordered compounds [17]. In $LiGaCr_4O_8$, the maximum around 55 K is associated with a short-range antiferromagnetic correlation in the paramagnetic phase, similar to that observed in the uniform pyrochlore lattice, for example, in $ZnCr_2O_4$ [32]. On the other hand, the maximum in magnetization around 60 K in $LiInCr_4O_8$ was initially attributed to opening of a spin gap [33], and it was later suggested, using time-of-flight neutron spectroscopy, that the spin gap is actually filled with magnetic states, thereby forming a pseudogap [16].

At low temperature (14.5 K), a first order long-range antiferromagnetic transition occurs in $LiGaCr_4O_8$, while in $LiInCr_4O_8$ a second order long-range antiferromagnetic ordering takes place around 13 K, as evident from the first derivative of magnetization with respect to temperature shown in the bottom inset of Figs. 3(a) and 3(b), respectively. In $ZnCr_2O_4$ the first order long-range antiferromagnetic ordering is coupled with the structural transition that occurs around 13 K. The first order nature of the antiferromagnetic ordering ($T_N \sim 14.5$ K) in the Ga compound is supported by thermal hysteresis in the temperature dependent field-cooled-cooling (FCC) and field-cooled-warming (FCW) magnetization data as shown in the upper inset of Fig. 3(a). This indicates that in the Ga compound, the magnetic ordering and the structural transition occur at the same temperature. A similar thermal hysteresis has been observed in $LiInCr_4O_8$ but at the structural phase transition temperature $T_S \sim 15.1$ K [upper inset of Fig. 3(b)] rather than at the magnetic phase transition temperature ($T_N \sim 13$ K), indicating that the antiferromagnetic ordering in the In compound is a conventional second order phase transition, consistent with a previous report [18].

The temperature dependent specific heat divided by temperature (C_p/T) measured on $LiGaCr_4O_8$ in zero magnetic field shows a λ-shaped anomaly at 14.1 K with a steplike feature at 14.5 K [Fig. 3(c)]. This could indicate that the structural and the magnetic transitions occur at different temperatures. On the contrary, an earlier report on this compound showed that the antiferromagnetic transition is coupled with the structural distortion, which is first order in nature [18]. In the present study, the close proximity of the two peak feature observed in the C_p/T data with an interval of 0.4 K makes it difficult to ascertain their origin. However, from the temperature dependent derivative of the dc magnetization [bottom inset Fig. 3(a)] and the thermal hysteresis in the C_p/T data [Fig. 3(c)], we suggest that the anomaly at 14.5 K could be due to the structural transition, and the magnetic ordering occurs at 14.1 K. To confirm this suggestion, we require further structural investigation across this temperature region. In a recent report by Lee *et al.*, it has been shown that the Ga compound undergoes magnetostructural and magnetic transitions at different temperatures, within an interval of 2.3 K [22]. The absence of any strong features in the C_p/T data around 55 K suggests that the entropy associated with the short-range spin-spin correlations in $LiGaCr_4O_8$ is small. In this context it is important to mention that the heat capacity data of $ZnCr_2O_4$ also do not show any anomaly at the short-range antiferromagnetic ordering [32].

In the case of $LiInCr_4O_8$, a sharp peak at 15.1 K and a change in slope around 13 K in the temperature dependent C_p/T data is evident in Fig. 3(d). In this compound, an interval of almost 2 K between the two anomalies makes it possible to distinguish the structural and magnetic transitions. Thermal hysteresis across the peak at 15.1 K [Fig. 3(d)] indicates the occurrence of a structural phase transformation at that temperature, while the change in slope around 13 K in the temperature dependent C_p/T data can be associated with the second order antiferromagnetic phase transition. This is further supported by the temperature dependent derivative of the dc magnetization data [bottom inset of Fig. 3(b)] of $LiInCr_4O_8$, which shows a peak at 15.1 K along with a

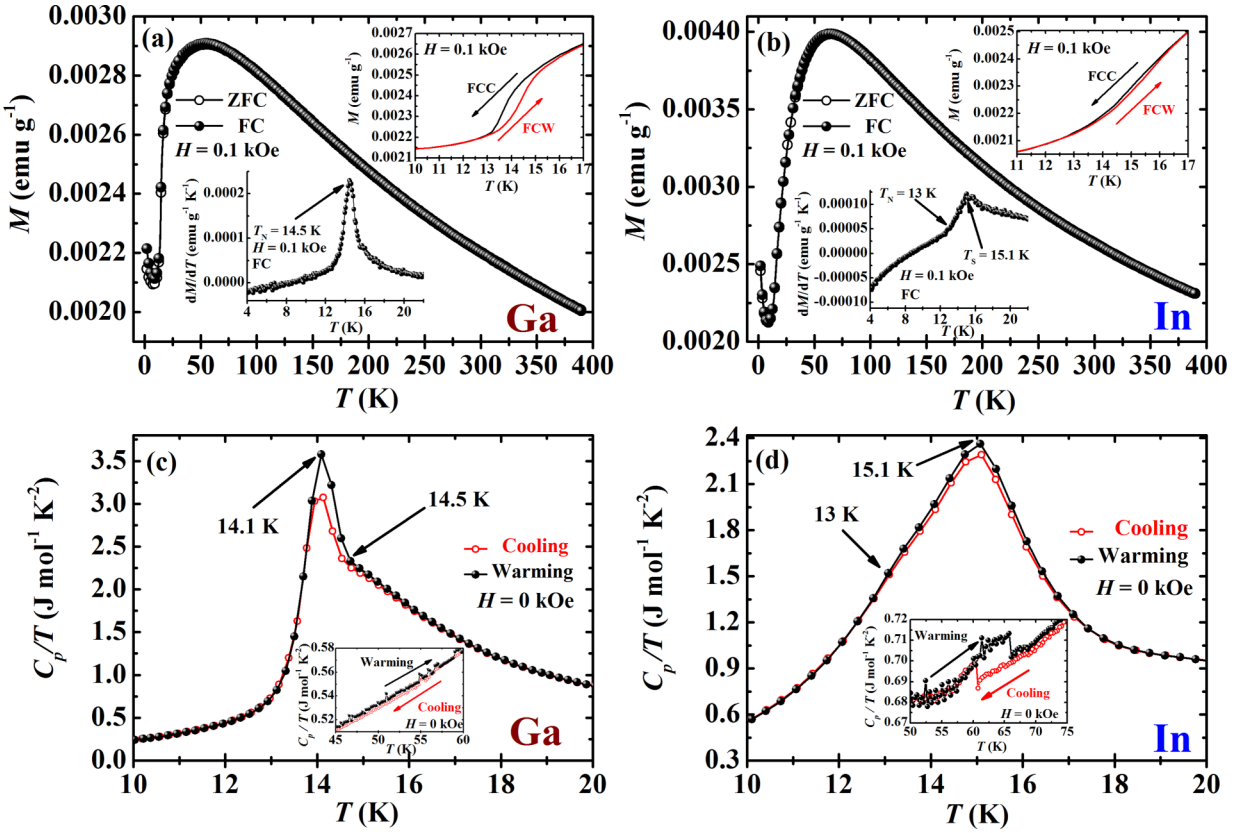

FIG. 3. (a, b) Temperature dependence of dc magnetization data of $LiGaCr_4O_8$ and $LiInCr_4O_8$, respectively, under zero-field-cooled (ZFC) and field-cooled (FC) conditions in the presence of a magnetic field of 0.1 kOe. Upper insets of panels (a) and (b) show the temperature dependent FCC and FCW magnetization data at 0.1 kOe, while the bottom insets of panels (a) and (b) show the first order derivative of magnetization with respect to temperature as a function of temperature at 0.1 kOe. (c, d) Temperature dependence of specific heat divided by temperature (C_p/T) for $LiGaCr_4O_8$ and $LiInCr_4O_8$ across T_N, respectively. Insets of panels (c) and (d) show the C_p/T data across short-range antiferromagnetic ordering ($T_{SO} \sim 55$ K) of the Ga compound and spin-gap opening temperature ($T_{SG} \sim 60$ K) of the In compound, respectively.

small anomaly at 13 K. Contrary to $LiGaCr_4O_8$, which does not show any anomaly in the C_p/T data in the vicinity of temperature where short-range antiferromagnetic ordering sets in [inset of Fig. 3(c)], $LiInCr_4O_8$ shows an anomaly and thermal hysteresis across the spin-gap opening temperature ($T_{SG} \sim 60$ K), as evident from the inset of Fig. 3(d). This observation is probably associated with the stronger breathing distortion in the In compound, indicating the presence of strong spin-lattice coupling. No significant effect of the magnetic field on the temperature dependent C_p/T data was observed in these compounds, indicating the robustness of the phase transition.

Now we discuss the results on the dielectric properties of $LiMCr_4O_8$ (M = Ga, In). Temperature dependent dielectric constants for the Ga and In compounds were measured in the temperature range of 7–100 K. For comparison, similar measurements were undertaken on $ZnCr_2O_4$, which shows a sharp dielectric anomaly in zero magnetic field at the first order antiferromagnetic phase transition ($T_N \sim 13$ K) [inset of Fig. 4(a)]. The appearance of a dielectric anomaly in the vicinity of the Néel temperature in zero magnetic field has been associated with a magnetostructural coupling induced by a spin Jahn-Teller effect [34]. The temperature dependent dielectric constant, measured in zero applied magnetic field for $LiGaCr_4O_8$, shows a strong dielectric anomaly at the magnetostructural phase transition temperature ($T_{MS} \sim 14.5$ K) and a broad anomaly in the vicinity of the short-range antiferromagnetic ordering temperature ($T_{SO} \sim 55$ K) [Fig. 4(a)]. For $LiInCr_4O_8$, dielectric anomalies appear both at the structural phase transition ($T_S \sim 15.1$ K) and spin-gap opening temperature ($T_{SG} \sim 60$ K) where the dielectric anomaly is very sharp compared with the Ga compound. It is important to note that the sharp feature of a dielectric anomaly at the spin gap strongly depends on the synthetic condition. $LiInCr_4O_8$ prepared at a higher annealing temperature ($\geqslant 1100$ °C), as well as repeated heating, led to the loss of Li. In such samples, no dielectric anomaly appears at the spin gap, indicating that a dielectric anomaly at the spin gap is sensitive to Li nonstoichiometry and disorder. Therefore, the present sample was prepared at a lower annealing temperature. In this context, we mention here that, in a recent paper, it has been shown that a broad feature appears in the temperature dependent dielectric data across the onset of the spin-gap transition [22].

Since the structural distortion in these compounds at low temperature leads to the coexistence of two crystallographic phases, which induces strain in the system due to lattice mismatch [30], the occurrence of a dielectric anomaly in both compounds in the vicinity of the Néel temperature, in zero magnetic field, could be attributed to the combined effect of structural phase coexistence and spin-lattice coupling via a magnetoelastic effect [35,36]. The structural phase

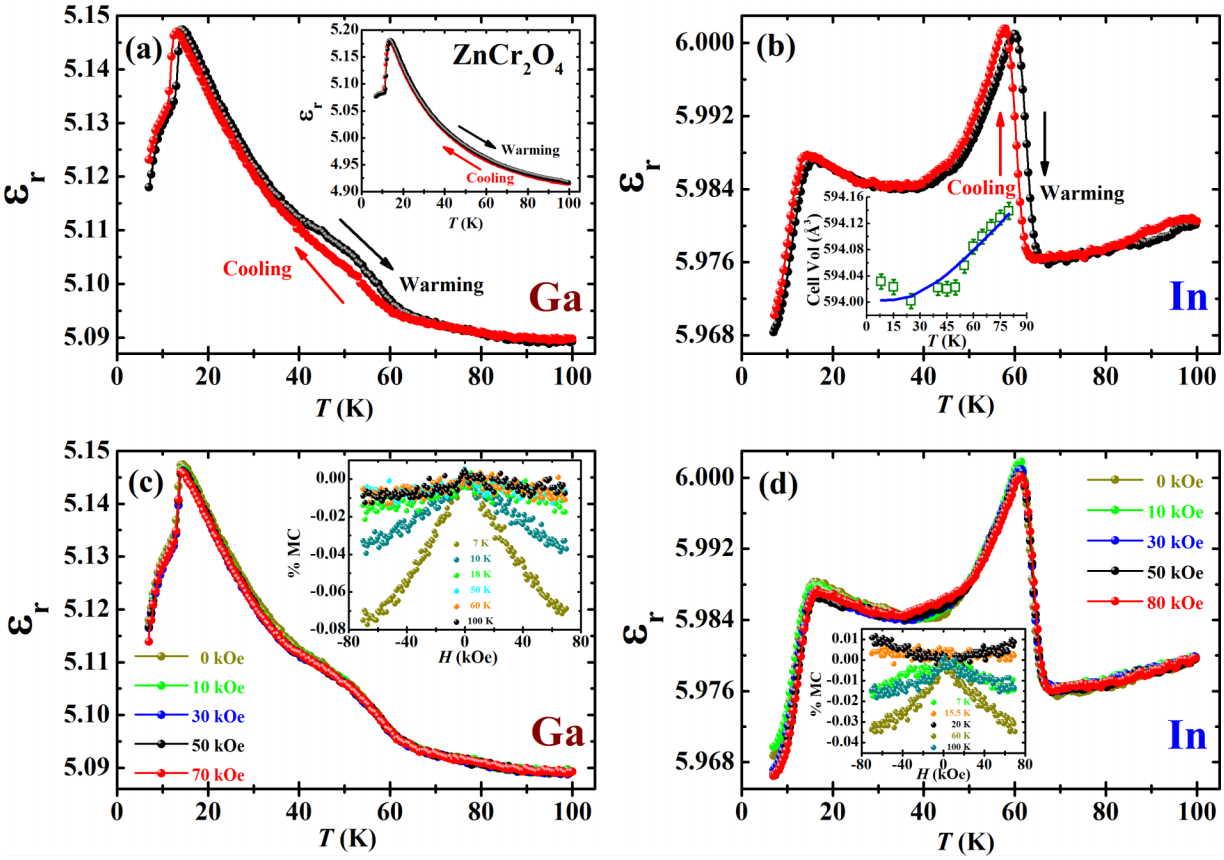

FIG. 4. (a, b) Temperature dependence of dielectric constant of $LiGaCr_4O_8$ and $LiInCr_4O_8$, respectively, in zero magnetic field at 50 kHz. Inset of panel (a) shows the temperature dependence of dielectric constant of $ZnCr_2O_4$ in zero magnetic field at 50 kHz. Inset of panel (b) shows the temperature dependent cell volume of the In compound fitted with a function of the type $V_0 = V_1 + V_2\theta_{S1}\text{Coth}\frac{\theta_{S1}}{T}$. The experimental data (square symbol) shows a discontinuity from the theoretical fit (blue line) at the spin gap, as well as magnetic and structural transitions (∼13–15 K). (c, d) Temperature dependence of dielectric constant of $LiGaCr_4O_8$ and $LiInCr_4O_8$, respectively, in the presence of different magnetic fields at 50 kHz. Insets of panels (c) and (d) show the magnetic field dependence magnetocapacitance (% MC) at 50 kHz for the Ga and In compounds, respectively.

coexistence and magnetoelastic effect gives rise to strain, which mediates the coupling between magnetization and the dielectric properties. The dielectric anomalies that appeared in the Ga and In compounds do not show frequency dependence. Both the Ga and In compounds show thermal hysteresis in the temperature dependent dielectric data measured across the magnetostructural ($T_{MS} \sim 14.5$ K) and structural phase transition ($T_S \sim 15.1$ K) temperatures, respectively, as shown in Figs. 4(a) and 4(b), indicating the first order nature of the phase transition associated with structural distortion. In addition, we also observe thermal hysteresis in the temperature dependent dielectric data across short-range antiferromagnetic ordering ($T_{SO} \sim 55$ K) and spin-gap opening temperature ($T_{SG} \sim 60$ K) in the Ga and In compound, respectively.

The difference between the dielectric anomalies in the Ga and In compounds across T_{SO} or T_{SG} can be understood by considering the Cr_4 breathing distortion, which is a unique feature of these *A*-site ordered chromate spinels. The breathing factors $[B_f = J'/J; (J > J')]$ are 0.1 for $LiInCr_4O_8$ and 0.6 for $LiGaCr_4O_8$ at room temperature, where J' and J correspond to the exchange integral on the large and small Cr_4 tetrahedra, respectively [17]. The higher breathing distortion in the In compound gives rise to a pseudogap in the magnetic excitation spectrum [16]. The existence of a gapped state in the In compound, due to the stronger breathing distortion, yields an additional contribution over the already existing spin-lattice coupling, thereby enhancing the dielectric anomaly in $LiInCr_4O_8$ at the spin-gap opening temperature ($T_{SG} \sim 60$ K). Although there is no change in the average structure across the spin gap, it is intriguing to note the anomaly in the temperature dependent cell volume in the vicinity of the spin gap, as shown in the inset Fig. 4(b). The temperature dependent cell volume was modeled with a function of the type $V_0 = V_1 + V_2\theta_{S1}\text{Coth}\frac{\theta_{S1}}{T}$, where θ_{S1} is the saturation temperature for the thermal expansion of the cubic structure [37]. The volume anomaly indicates a local structural change induced by the opening of a spin gap. The anomaly in cell volume at the magnetostructural transition at low temperature (∼15 K) can also be seen in the same figure. Conversely, in $LiGaCr_4O_8$, the origin of the broad dielectric anomaly that accompanies the short-range antiferromagnetic ordering ($T_{SO} \sim 55$ K) can only be associated with spin-lattice coupling, due to the weak breathing distortion. The importance of the breathing distortion in inducing a dielectric anomaly in $LiMCr_4O_8$ (M = Ga, In) at T_{SO} or T_{SG} is further supported by the absence of a dielectric anomaly [inset of Fig. 4(a)]

in the conventional chromate spinel ($ZnCr_2O_4$), where a breathing distortion is absent due to equivalent Cr-Cr distance. A dielectric anomaly at the spin-gap temperature has seldom been reported in the literature. It may be mentioned here that a dielectric anomaly has been observed in NaV_2O_5 at the spin-gap opening temperature in the high frequency region, and this anomaly has been attributed to the antiferroelectric charge ordering, in the form of a zigzag arrangement of V^{4+} ions [38].

To probe the effect of a magnetic field on the dielectric properties of *A*-site ordered chromate spinels, temperature dependent dielectric constants were measured in the presence of various magnetic fields [Figs. 4(c) and 4(d)]. There is no significant effect of magnetic field on the overall dielectric constant of $LiGaCr_4O_8$, except for a small shift of the dielectric peak to the higher temperature with increasing magnetic field, as evident from Fig. 4(c). Measurement of the isothermal magnetocapacitance (% MC) for the Ga compound as a function of magnetic field shows that below the Néel temperature ($T_N \sim 14.5$ K), the magnetocapacitance (% MC) has reached the maximum value of 0.08% at 7 K, and it remains low above the magnetic ordering temperature, as shown in the inset of Fig. 4(c). Application of a magnetic field has little impact on the dielectric behavior of $LiInCr_4O_8$, other than a small shift of both the dielectric peaks to higher temperature with increasing magnetic fields, as shown in Fig. 4(d). The inset of Fig. 4(d) illustrates that near the spin-gap opening temperature ($T_{SG} \sim 60$ K), the magnetocapacitance (% MC) reaches a maximum value of 0.04%, while at other temperatures it remains almost negligible. The observed values of the magnetocapacitance (% MC) in these two compounds are comparable to those observed in other chromate spinel oxides containing magnetic ions at the *A* site [39]. The observed shift in the dielectric peak with magnetic field could be attributed to the coupling between the dielectric response and q-dependent spin-spin correlation, where spin-spin correlations soften the optical phonon frequency, giving rise to a shift in the dielectric peak, according to the Lyddane-Sachs-Teller relation [40–42].

Measurement of the pyroelectric current of these compounds, in the presence of various magnetic fields, did not reveal a pyroelectric peak. Moreover, since there is no significant effect of magnetic fields on the dielectric constant of either $LiGaCr_4O_8$ or $LiInCr_4O_8$, we suggest that the effect of magnetic field in inducing magnetoelectric current, if any, would be very small. The absence of linear magnetoelectric polarization is consistent with the observed magnetic structures of $LiGaCr_4O_8$, which do not allow linear magnetoelectric effects. However, since these crystals are piezoelectric, they should possess a second order magnetoelectric effect irrespective of magnetic ordering, which is probably quite small.

IV. CONCLUSIONS

The present study clearly demonstrates the magnetodielectric effect in the *A*-site ordered chromate spinel where dielectric anomalies appear in the vicinity of long-range as well as short-range (or spin-gap) antiferromagnetic ordering temperatures. The origin of a dielectric anomaly near T_N has been attributed to the combined action of a spin Jahn-Teller effect via strong spin-lattice coupling and strain that arises due to structural phase coexistence, signifying the role of a complex magnetostructural effect. In addition to the already existing spin-lattice interaction, the existence of a gapped state enhances the dielectric anomaly feature at higher temperatures in the In compound compared with the Ga compound without any gapped state. Therefore introduction of breathing distortion provides additional degrees of freedom in the geometrically frustrated pyrochlore lattice to explore many interesting properties.

ACKNOWLEDGMENTS

A.S. acknowledges financial support from Science and Engineering Research Board (SERB; Sanction No. EMR/2014/000896), Department of Science & Technology, Government of India, and Sheikh Saqr Laboratory at Jawaharlal Nehru Centre for Advanced Scientific Research (JNCASR). The work at Sydney University is supported by the Australian Research Council (Grant No. DP150102863). R.S. and A.S. acknowledge N. V. Ter-Oganessian from Southern Federal University, Russia, for valuable discussions. R.S. acknowledges JNCASR for providing a research fellowship.

[1] W. Eerenstein, N. D. Mathur, and J. F. Scott, Nature **442**, 759 (2006).
[2] Y. Tokura and S. Seki, Adv. Mater. **22**, 1554 (2010).
[3] J. Scott, J. Mater. Chem. **22**, 4567 (2012).
[4] C. N. R. Rao, A. Sundaresan, and R. Saha, J. Phys. Chem. Lett. **3**, 2237 (2012).
[5] M. C. Kemei, P. T. Barton, S. L. Moffitt, M. W. Gaultois, J. A. Kurzman, R. Seshadri, M. R. Suchomel, and Y.-I. Kim, J. Phys.: Condens. Matter **25**, 326001 (2013).
[6] M. Matsuda, M. Takeda, M. Nakamura, K. Kakurai, A. Oosawa, E. Lelièvre-Berna, J.-H. Chung, H. Ueda, H. Takagi, and S.-H. Lee, Phys. Rev. B **75**, 104415 (2007).
[7] J. B. Goodenough, Phys. Rev. **117**, 1442 (1960).
[8] S.-H. Lee, C. Broholm, W. Ratcliff, G. Gasparovic, Q. Huang, T. Kim, and S.-W. Cheong, Nature **418**, 856 (2002).
[9] A. Ramirez, Annu. Rev. Mater. Sci. **24**, 453 (1994).
[10] Y. Yamashita and K. Ueda, Phys. Rev. Lett. **85**, 4960 (2000).
[11] O. Tchernyshyov, R. Moessner, and S. L. Sondhi, Phys. Rev. Lett. **88**, 067203 (2002).
[12] S. Bordács, D. Varjas, I. Kézsmárki, G. Mihály, L. Baldassarre, A. Abouelsayed, C. A. Kuntscher, K. Ohgushi, and Y. Tokura, Phys. Rev. Lett. **103**, 077205 (2009).
[13] M. C. Kemei, S. L. Moffitt, L. E. Darago, R. Seshadri, M. R. Suchomel, D. P. Shoemaker, K. Page, and J. Siewenie, Phys. Rev. B **89**, 174410 (2014).
[14] V. Kocsis, S. Bordács, D. Varjas, K. Penc, A. Abouelsayed, C. A. Kuntscher, K. Ohgushi, Y. Tokura, and I. Kézsmárki, Phys. Rev. B **87**, 064416 (2013).
[15] S. Lee, A. Pirogov, Misun Kang, Kwang-Hyun Jang, M. Yonemura, T. Kamiyama, S.-W. Cheong, F. Gozzo, Namsoo Shin, H. Kimura, Y. Noda, and J.-G. Park, Nature **451**, 805 (2008).

[16] G. J. Nilsen, Y. Okamoto, T. Masuda, J. Rodriguez-Carvajal, H. Mutka, T. Hansen, and Z. Hiroi, Phys. Rev. B **91**, 174435 (2015).
[17] Y. Okamoto, G. J. Nilsen, J. P. Attfield, and Z. Hiroi, Phys. Rev. Lett. **110**, 097203 (2013).
[18] Y. Tanaka, M. Yoshida, M. Takigawa, Y. Okamoto, and Z. Hiroi, Phys. Rev. Lett. **113**, 227204 (2014).
[19] N. V. Ter-Oganessian, J. Magn. Magn. Mater. **364**, 47 (2014).
[20] V. P. Sakhnenko and N. V. Ter-Oganessian, J. Phys.: Condens. Matter **24**, 266002 (2012).
[21] R. Saha, S. Ghara, E. Suard, D. H. Jang, K. H. Kim, N. V. Ter-Oganessian, and A. Sundaresan, Phys. Rev. B **94**, 014428 (2016).
[22] S. Lee, S.-H. Do, W.-J. Lee, Y. S. Choi, M. Lee, E. S. Choi, A. P. Reyes, P. L. Kuhns, A. Ozarowski, and K.-Y. Choi, Phys. Rev. B **93**, 174402 (2016).
[23] N. V. Ter-Oganessian (private communication).
[24] J. Rodríguez-Carvajal, Physica B: Condens. Matter **192**, 55 (1993).
[25] F. Fauth, I. Peral, C. Popescu, and M. Knapp, Powder Diffr. **28**, S360 (2013).
[26] F. Fauth, R. Boer, F. Gil-Ortiz, C. Popescu, O. Vallcorba, I. Peral, D. Fullà, J. Benach, and J. Juanhuix, Eur. Phys. J. Plus **130**, 1 (2015).
[27] K.-D. Liss, B. Hunter, M. Hagen, T. Noakes, and S. Kennedy, Physica B: Condensed Matter **385**, 1010 (2006).
[28] E. Verwey and E. Heilmann, J. Chem. Phys. **15**, 174 (1947).
[29] M. Weil and B. Stöger, Acta Crystallogr. Sec. E **62**, i199 (2006).
[30] M. C. Kemei, J. K. Harada, R. Seshadri, and M. R. Suchomel, Phys. Rev. B **90**, 064418 (2014).
[31] E. F. Bertaut, *Magnetism*, edited by G. T. Rado and H. Shull (Academic Press, New York, 1963), Vol. III, Chap. 4, pp. 149–209.
[32] H. Martinho, N. O. Moreno, J. A. Sanjurjo, C. Rettori, A. J. García-Adeva, D. L. Huber, S. B. Oseroff, W. Ratcliff, II, S.-W. Cheong, P. G. Pagliuso, J. L. Sarrao, and G. B. Martins, Phys. Rev. B **64**, 024408 (2001).
[33] Y. Okamoto, G. J. Nilsen, T. Nakazono, and Z. Hiroi, J. Phys. Soc. Jpn. **84**, 043707 (2015).
[34] I. Kagomiya, H. Sawa, K. Siratori, K. Kohn, M. Toki, Y. Hata, and E. Kita, Ferroelectrics **268**, 327 (2002).
[35] C. dela Cruz, F. Yen, B. Lorenz, Y. Q. Wang, Y. Y. Sun, M. M. Gospodinov, and C. W. Chu, Phys. Rev. B **71**, 060407(R) (2005).
[36] T. Suzuki and T. Katsufuji, J. Phys.: Conf. Series **150**, 042195 (2009).
[37] B. J. Kennedy, I. Qasim, and K. S. Knight, J. Phys.: Condens. Matter **27**, 365401 (2015).
[38] A. I. Smirnov, M. N. Popova, A. B. Sushkov, S. A. Golubchik, D. I. Khomskii, M. V. Mostovoy, A. N. Vasil'ev, M. Isobe, and Y. Ueda, Phys. Rev. B **59**, 14546 (1999).
[39] N. Mufti, A. Nugroho, G. Blake, and T. Palstra, J. Phys.: Condens. Matter **22**, 075902 (2010).
[40] T. Katsufuji and H. Takagi, Phys. Rev. B **64**, 054415 (2001).
[41] U. Adem, L. Wang, D. Fausti, W. Schottenhamel, P. H. M. van Loosdrecht, A. Vasiliev, L. N. Bezmaternykh, B. Büchner, C. Hess, and R. Klingeler, Phys. Rev. B **82**, 064406 (2010).
[42] G. Lawes, A. P. Ramirez, C. M. Varma, and M. A. Subramanian, Phys. Rev. Lett. **91**, 257208 (2003).